Innovative Octave Band Quad Ridge Feed Horn and Vacuum Window for Next-Generation Radio Observatories

S. Salem Hesari[1,2], N. Tasouji[2], I. Wevers[1], V. Reshetov[1], J. Bornemann[2], L. Knee[1], A. Densmore[1]

[1] NRC Herzberg Astronomy and Astrophysics Research Centre, Victoria, BC, Canada

[2] Department of Electrical and Computer Engineering, University of Victoria, Victoria, BC, Canada

ABSTRACT

In the effort to push the boundaries of radio astronomy observations, technological innovations are essential for future generations of observatories. This paper introduces an innovative design for future radio receivers in major observatories like ngVLA, ALMA, and SKA. The concept centers around an Octave Band Quad Ridge Feed Horn and Vacuum Window, designed to operate within the 25 to 50 GHz (2:1) frequency range. This cutting-edge feed model uses dielectric loading to enhance phase and polarization efficiency, thereby significantly increasing the overall aperture efficiency across the bandwidth. The dielectric rod, features a solid construction with comb-shaped ridges located in the throat of the feed horn. To complete the entire optic model an HDPE vacuum window with three custom designed antireflection layers to minimize the signal reflections, is designed and presented. To confirm the performance of the proposed model, we use two different 3D full-wave electromagnetic simulators, CST Studio Suite and HFSS. The results showcase a return loss exceeding 25dB with exceptional beam symmetry across the entire bandwidth.

Keywords: Wideband receiver, ngVLA, cryogenic receiver, feed horn, Vacuum Window, Octave band, Quad ridge.

1. INTRODUCTION

The instantaneous bandwidth accessible to mm-wave radio astronomy receivers limits both the sensitivity of continuum observations as well as the volume of spectral data collected. Traditional technologies have limited the bandwidth to less than an octave, constraining the scope of scientific research. However, recent advancements in technology are paving the way to potentially expand these limits [1], [2], [3], [4], [5], [6], [7], [8], [9], [10]. These innovations could lead to the creation of wideband mm-wave systems that are capable of covering an entire octave or even more, significantly increasing the scientific productivity of radio observatories. Such enhancements in mm-wave receivers promise to improve both existing and forthcoming radio observatories, including major projects like ALMA, SKA, and the ngVLA.

The wideband receivers, particularly those operating in the octave band (2:1 frequency ratio), offer important benefits over standard band receivers (1.67:1 frequency ratio). One of the primary advantages is cost efficiency. By using octave band receivers, fewer units are required to achieve complete frequency coverage, which is especially advantageous for expansive telescope arrays like the ngVLA, SKA, and ALMA. Moreover, octave band receivers facilitate wideband observations and significantly enhance sensitivity for continuum measurements. Given these advantages, octave band radio receivers are highly valued in millimetre-wave radio astronomy, enabling more dynamic and cost-effective exploration of the universe.

This paper concentrates on the design and development of crucial components for octave band front-end receivers, specifically the feed horn and the vacuum window. We propose a novel octave band dielectrically loaded quad ridge feed horn, known for its broad bandwidth and dual-polarization capabilities, enabling it to capture a wide range of frequencies [1]. Additionally, we introduce an octave band vacuum window model, made from high-density polyethylene (HDPE), which protects sensitive telescope elements while maintaining signal integrity and cryogenic temperatures. Designed to be transparent to radio waves, the vacuum window ensures minimal attenuation of incoming signals [11], [12].

2. QUAD RIDGE FEED HORN

This section presents a dielectrically loaded octave band quad ridge feed horn, tailored specifically for the ngVLA's optical requirements. The design ensures a feed pattern with a 16 dB edge taper at a 55° opening half-angle, consistent with the specifications outlined in the ngVLA reference design [13]. This feed horn is engineered to optimally illuminate the shaped offset Gregorian reflector.

Designing a wideband quad ridge feed horn presents significant challenges, particularly in maintaining beam symmetry across a wide bandwidth. While the ridge structure inherently provides excellent reflection loss over a wide bandwidth, the beamwidth tends to narrow at higher frequencies. To address this issue, a dielectric rod has been incorporated into the design. This rod plays a crucial role in controlling and stabilizing the beamwidth across the entire frequency band, ensuring consistent performance.

This feed is designed to operate in the frequency range of 25-50GHz, with a return loss better than 25dB for a bandwidth ratio of 2:1. The feed horn structure and reflection loss is shown in Figure 1. The quad ridge feed is designed in a way to only excite the dominant mode and keep all higher order modes below -70dB across the bandwidth which reduces the chances of exciting higher modes when the feed gets connected to other components of the receiver.

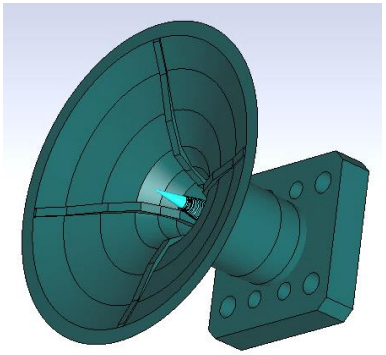

(a)

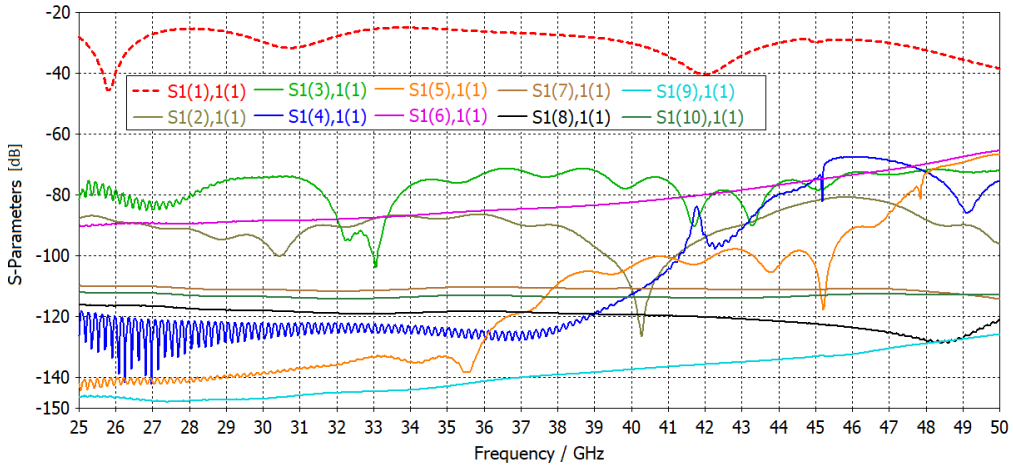

(b)

Figure 1. Dielectrically loaded quad ridge feed horn: (a) structure of the feed horn, (b) S-parameters of the feed horn, including the first 10 excited modes, simulated in CST.

To achieve a symmetric radiation pattern across the bandwidth, the feed structures are carefully designed and optimized using Genetic algorithm. Additionally, a HDPE dielectric rod with comb-shaped corrugations is designed to enhance the rotational symmetry of the radiation pattern around the phase centre. Visualizations of the electric field distribution within the feed horn, along with a 3D model of the radiation pattern at 35 GHz, are presented in Figure 2. Figure 3 presents the radiation pattern of the feed at 0, 45, and 90 degrees (E-plane, diagonal plane, and H-plane) across the bandwidth from 25 to 50 GHz with 1GHz frequency steps across the band, simulated in CST. These illustrations highlight the design's effectiveness in achieving uniform and symmetric radiation patterns over a wide bandwidth.

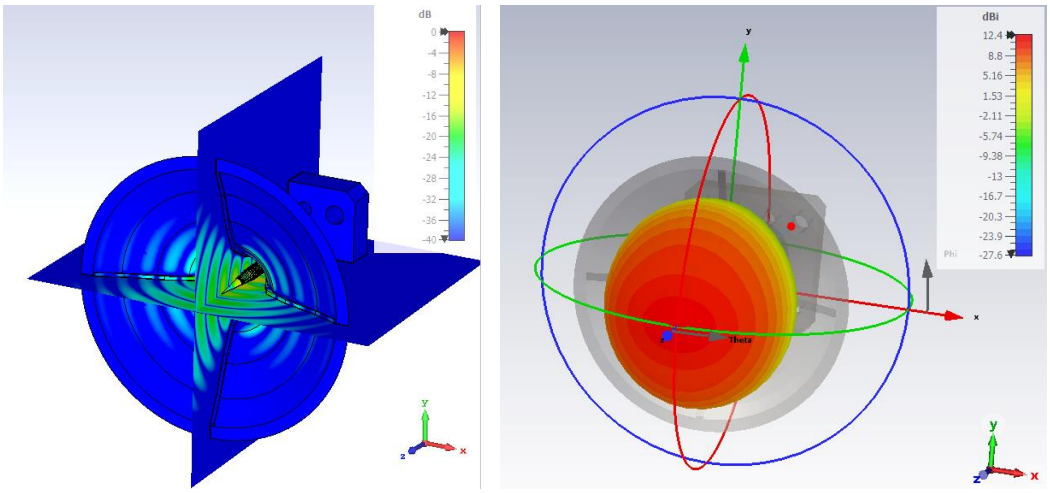

(a) (b)

Figure 2. (a) Electric field distribution within the feed horn at 35GHz, (b) 3D model of the radiation pattern at 35GHz, simulated in CST.

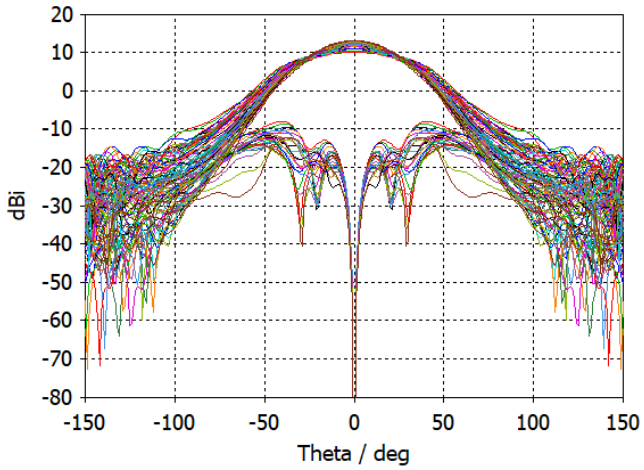

Figure 3. Radiation pattern of the quad ridge feed horn in the E, H, and D-planes across the bandwidth 25-50GHz with 1GHz frequency step, simulated CST.

To assess the performance of the feed horn, we employed two distinct electromagnetic (EM) full-wave simulators that utilize different numerical methods: CST Studio Suite and HFSS. In CST, the feed was modeled and analyzed in the time domain using the Finite Integration Technique (FIT), while HFSS employs the Finite Element Method (FEM) for solving electromagnetic problems. The simulation results from HFSS are in excellent agreement with those from CST, as demonstrated in Figure 4 and 5.

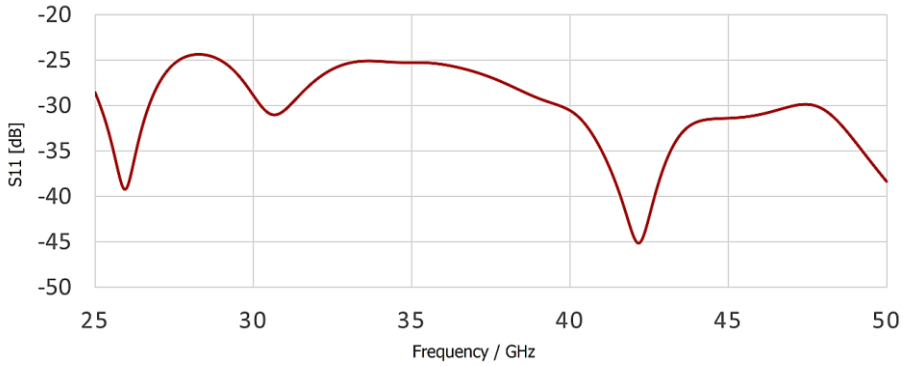

Figure 4. HFSS simulated reflection loss of the octave band quad ridge feed horn.

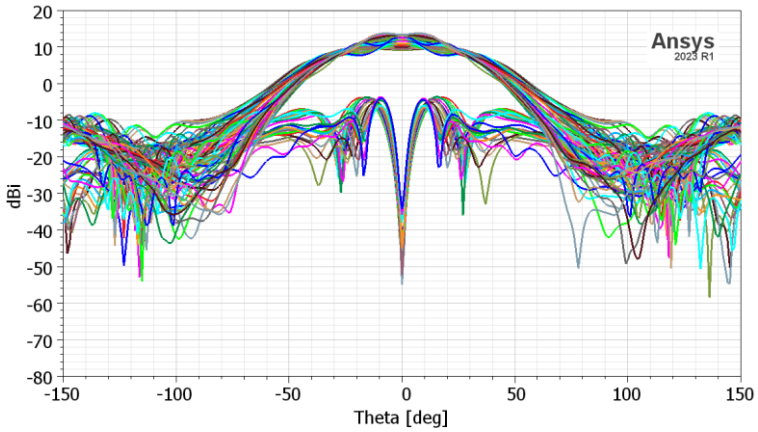

Figure 5. HFSS simulated radiation pattern of the quad ridge feed horn at E, H, and D-planes across the bandwidth 25-50GHz with 1GHz frequency step.

The aperture efficiency of the feed horn, is calculated considering a prime focus reflector dish featuring an f/D ratio of 0.42. The calculation of the aperture efficiency integrates several key performance metrics, including amplitude, polarization, phase, and spillover efficiencies, from established methodologies discussed in [14], [15].

To achieve a detailed and accurate evaluation of efficiencies, we adopt the equivalent paraboloid equations that have been articulated in [16] to provide a framework for assessing the capabilities of our feed horn within its operational bandwidth. Our analysis demonstrates that the feed horn achieves an average aperture efficiency about 80% across the bandwidth and it maintains an excellent phase efficiency, exceeding 99.5% from 25-50 GHz, shown in Figure 6.

Since the ngVLA employs a dual-shaped reflector offset Gregorian configuration, the aperture efficiency achievable with ngVLA optics is expected to be significantly higher than the values calculated here, which are based on a simpler single Cassegrain dish. For future work, we plan to conduct an optical analysis using the ngVLA Cycle 7 optics to determine the accurate aperture efficiency. Preliminary calculations for a fairly similar feed system are presented in [1], indicating an aperture efficiency exceeding 91.3% across the band.

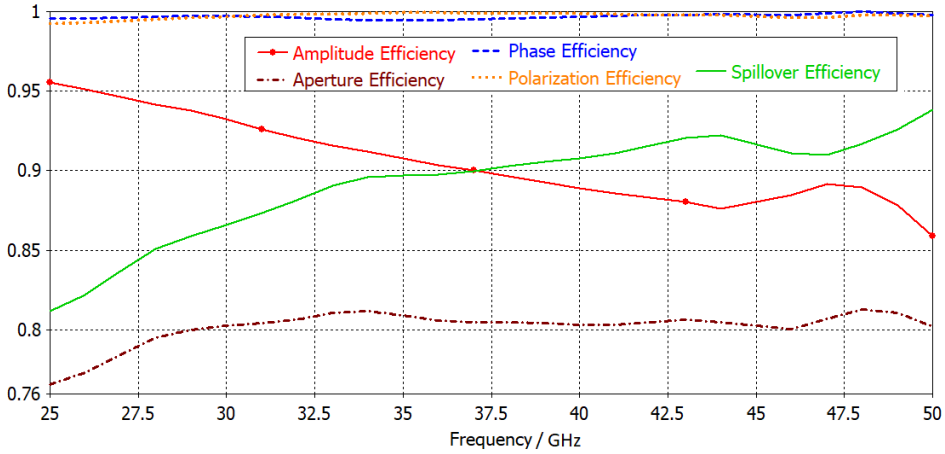

Figure 6. Efficiencies of the octave band quad ridge feed horn across the bandwidth.

3. VACUUM WINDOW

The vacuum window plays a key role in defining the noise temperature of the radio receiver cartridge used in radio astronomy applications. As the initial optical component in the receiver chain, its influence on the overall system performance is significant. Consequently, a careful analysis, calculation, and measurement of the vacuum window's noise contribution are essential. This process guarantees that the vacuum window has minimal loss and maximizes efficiency, thus enhancing the receiver's performance and ensuring optimal system sensitivity overall.

To achieve a wideband vacuum window with minimal loss, a design featuring a three-layered antireflection coating on a solid piece of HDPE has been developed. This multilayer antireflection approach enhances the transmissive properties of the window by reducing reflections at the interface between air and the HDPE substrate [17]. Each layer is carefully designed to optimize the phase and amplitude of incoming light across a broad spectrum, ensuring maximum transmission and minimal signal loss. Using three stepped circular antireflection layers not only improves the overall efficiency of the vacuum window but also extends its operational bandwidth, making it highly effective for radio astronomy applications.

Figure 7 illustrates the configuration and performance of the designed antireflection layers applied to both sides of a solid HDPE layer. As shown, this design achieves a reflection loss greater than 30dB across the bandwidth. Additionally, the insertion loss of the proposed model averages approximately -0.005 dB throughout the band.

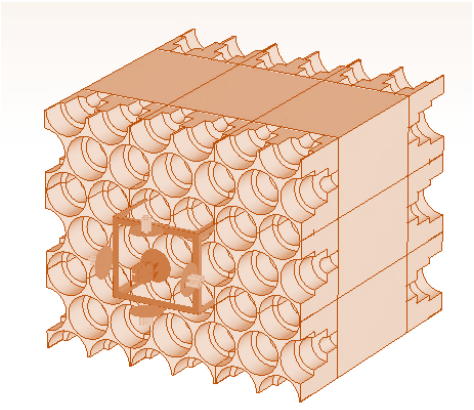

(a)

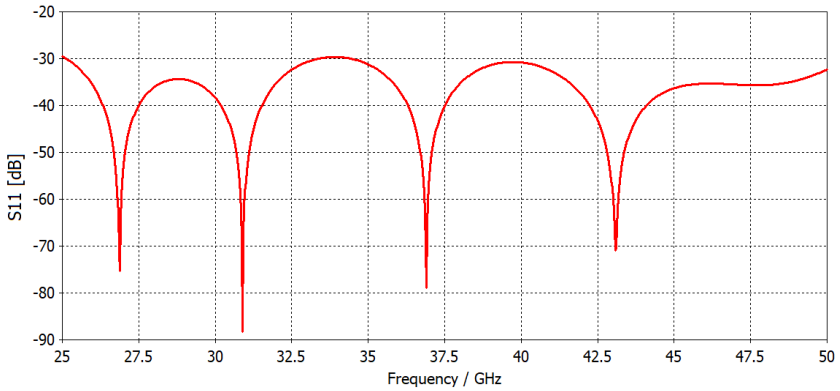

(b)

Figure 7. (a) Three layered antireflection coating for the proposed vacuum window, (b) reflection loss of the HDPE window including antireflections layers on both sides.

We implemented the above-mentioned antireflection layer in designing an octave band vacuum window, utilizing the suggested top-hat structure in [18] to minimize truncations and additional losses. Figure 8 displays the window's structure, which includes assembly rings, screws, and pins.

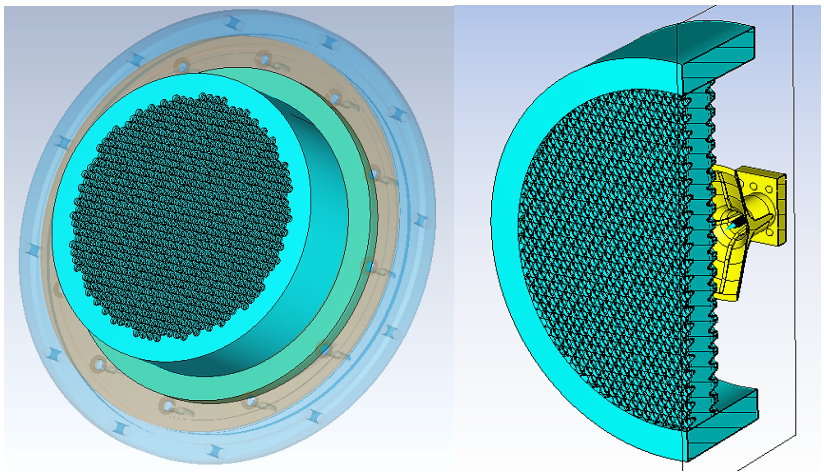

Figure 8. Octave band vacuum window configuration.

The electromagnetic analysis conducted in CST shows the performance of the vacuum window placed in front of the feed horn. The reflection loss data shown in Figure 9 demonstrate that the vacuum window has a minimal effect on feed performance. Additionally, we recalculated the efficiencies for the feed horn in conjunction with the vacuum window to assess its impact. As depicted in Figure 10, the introduction of this vacuum window does not degrade feed performance, with discrepancies proving to be negligible.

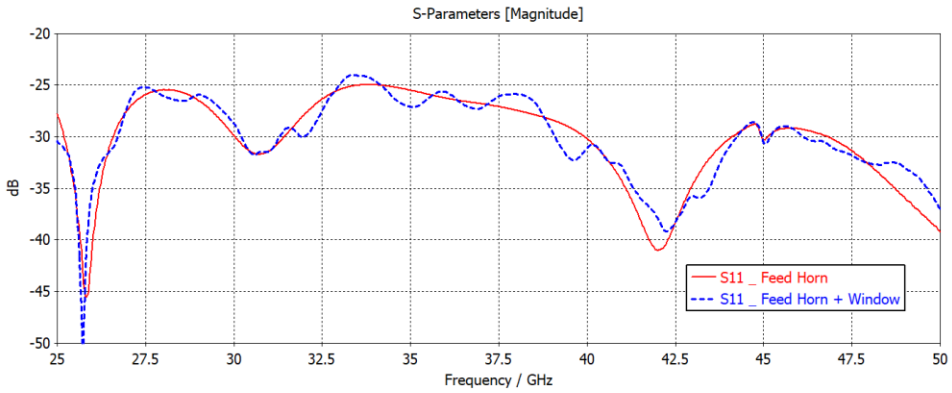

Figure 9. Octave band vacuum window reflection loss across the bandwidth.

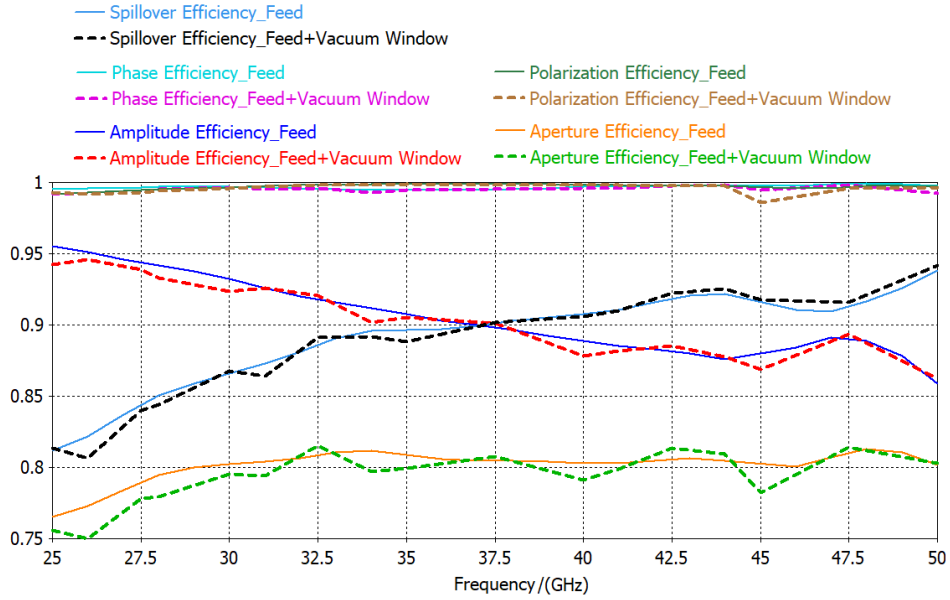

Figure 10. Efficiencies of the octave band vacuum window across the bandwidth.

4. MECHANICAL ANALYSIS OF THE OCTAVE BAND VACUUM WINDOW

6.1 Stress Analysis of HDPE Window with Antireflection Pattern

A static Finite Element Analysis (FEA) was performed using ANSYS 22 to evaluate the structural integrity of an 18 mm thick HDPE window. The specific dimensions and design details of the window are illustrated in Figures 11, 12, and 13. This analysis aimed to assess the stress distribution across the window under typical loading conditions This stress level is significantly below the recommended safety threshold of 5 MPa (Figure 14) for the lowest grade of HDPE material, indicating a robust safety margin. The results indicated that the maximum stress experienced by the window reached 3.6 MPa, shown in Figure 15.

Additionally, we conducted calculations to determine the maximum deflection of the vacuum window under atmospheric pressure, which was found to be 0.213 mm. This calculation, detailed in Figure 16, reflects the structural response of the window when subjected to the external pressure, highlighting its robustness and suitability for the operational environment. This assessment ensures that the vacuum window maintains its integrity and performance under typical atmospheric conditions.

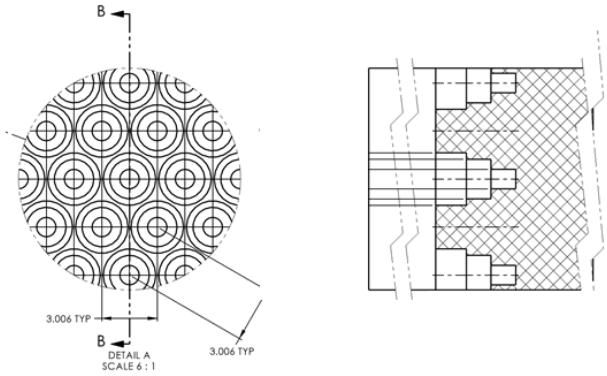

Figure 11. Geometry of the vacuum window pattern.

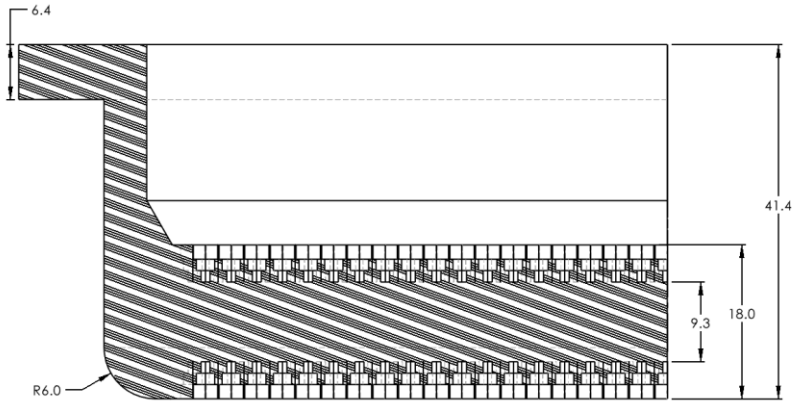

Figure 12. Cross-section view of the window.

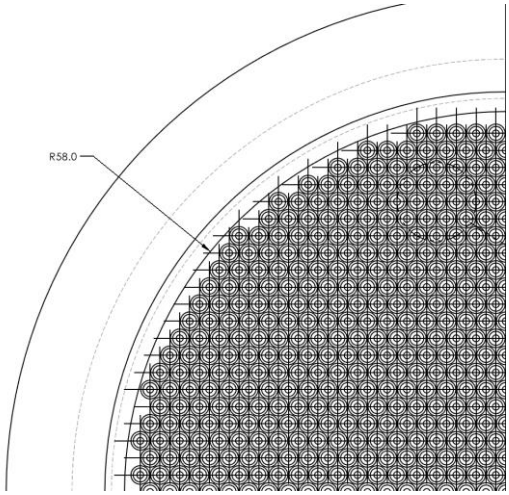

Figure 13. Front segment view of the window.

The maximum permissible stress level of 5 MPa and a safety factor of 1.26 are based on established standards for water piping systems. These standards are applicable because the material in question, HDPE, commonly used in the manufacture

of water pipes, requires rigorous stress-resistance properties to withstand internal water pressure and external environmental factors. This correlation ensures that when the material is adapted for other applications, such as in HDPE vacuum windows with antireflection patterns, it maintains a high level of durability and safety under similar stress conditions.

It's important to recognize that HDPE behaves as a visco-elastic material, meaning the deflection of the window varies over time. The Finite Element Analysis (FEA) was performed using the initial elastic modulus (at time = 0) [11]. Since deflection is directly proportional to the apparent elastic modulus, we can estimate the maximum deflection over time, as shown in Table 1. This deflection over time was also modeled using ANSYS, with results depicted in Figure 17.

Table 1. Maximum deflection of the window vs. time.

Time	Apparent elastic modulus, [MPa]	Elastic modulus relative to time 0	Max Deflection, [mm]
0	1035	100%	0.213
1000 h	303	29.3%	0.75
1 year	262	25.3%	0.87
10 years	221	22%	1.0

Design Stress and Safety Factor (service factor)

Safety factors take into account handling conditions, service conditions and other circumstances not directly considered in the design. In terms of SABS ISO 4427 the minimum safety factor is 1.25. This factor, when applied to the Minimum Required Strength (MRS), for the particular material classification (e.g. PE80, PE100), gives the maximum allowable hydrostatic design stress for the designated material.

Designation of material	MRS at 50 years and 20°C Mpa	Maximum allowable hydrostatic design stress, σ – Mpa
PE 100	10	8
PE 80	8	6.3
PE 63	6.3	5

The table below illustrates the relationship between MRS and σ for various design coefficients at 20° C.

Hydrostatic design stress of pipe, σ - MPa	MRS of material - MPa		
	10	8	6.3
	Design coefficient, C		
8	1.25		
6,3	1.59	1.27	
5	2	1.6	1.26

Figure 14. Design stress and safety factors for HDPE [11].

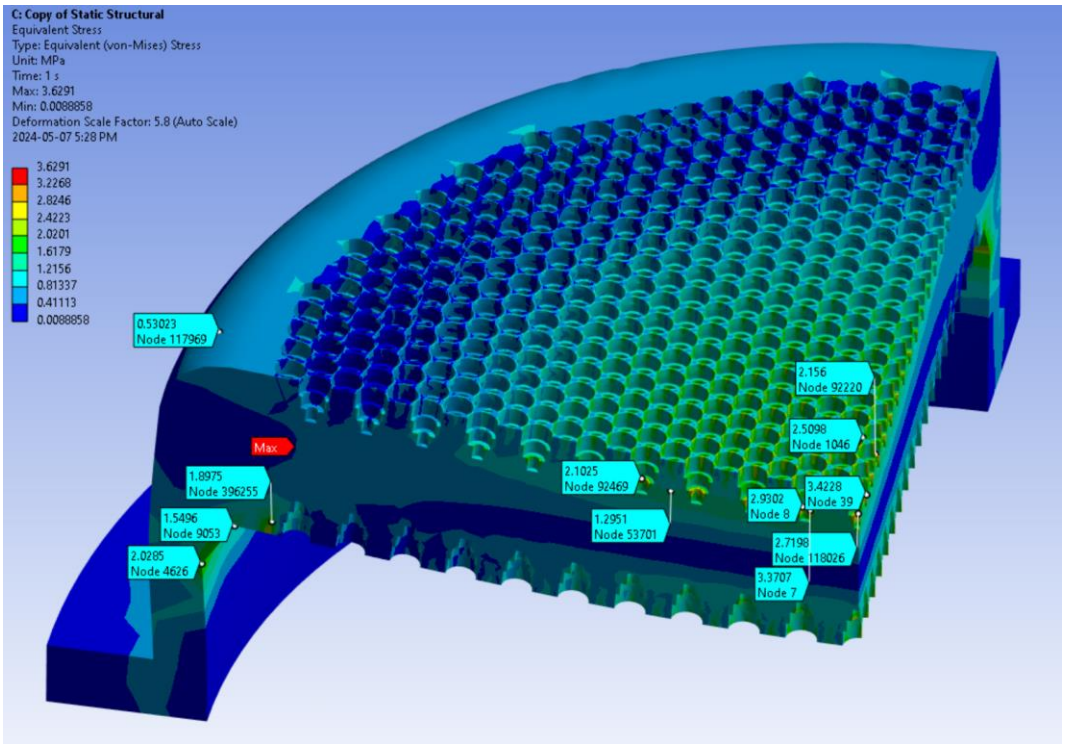

Figure 15. FEA stress results, with maximum equivalent stress of 3.6 MPa.

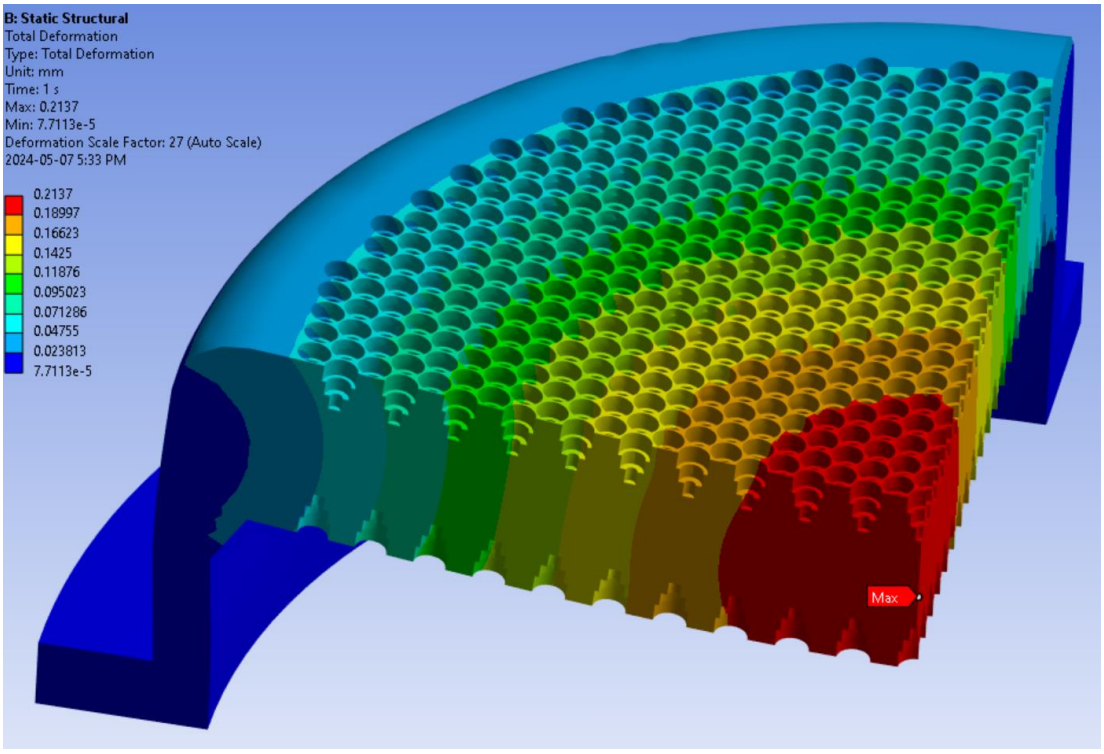

Figure 16. Maximum instantaneous deflection of the window under atmospheric pressure is 0.213 mm.

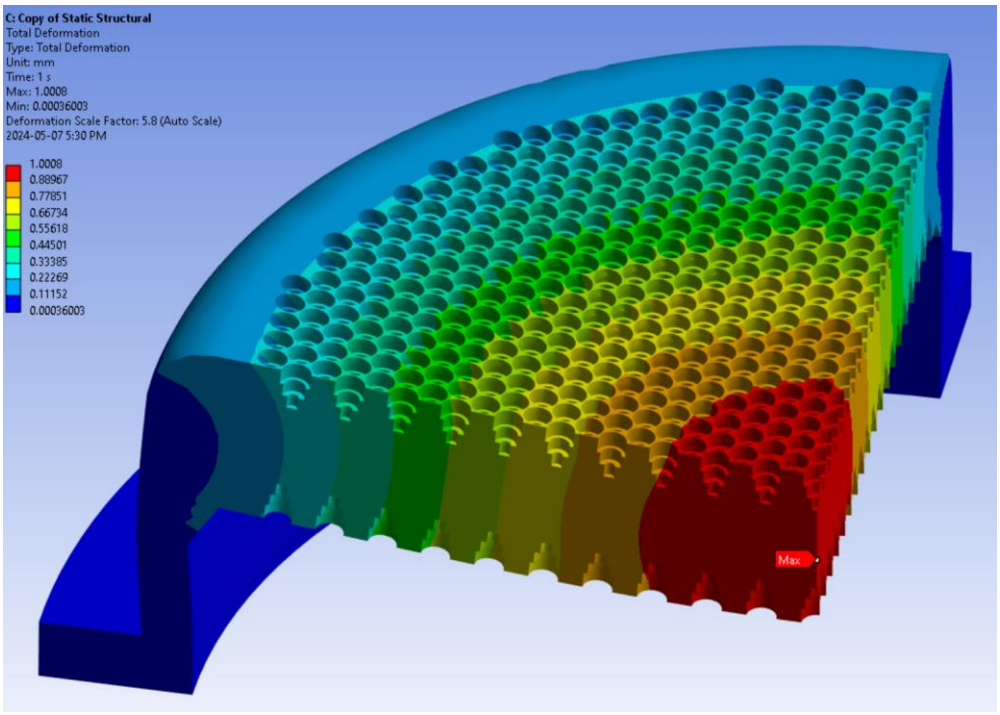

Figure 17. Maximum deflection of the window in 10-year time.

5. REFERENCES

[1] S. Salem Hesari, B. Veidt and I. Wevers, "A Compact Dielectrically Loaded Quad-ridge Feed Horn for Octave Band Radio Astronomy Application," in *32nd IEEE International Symposium on Space THz Technology (ISSTT 2022)*, Baeza, Spain, October 16-20, 2022.

[2] D. Henke, F. Jiang, S. Salem Hesari, A. Seyfollahi, B. Veidt and L. B. G. Knee, "Octave bandwidth receiver technology for radio and millimetre-wave telescopes," in *Proc. SPIE 12190, Millimeter, Submillimeter, and Far-Infrared Detectors and Instrumentation for Astronomy XI, 121901Y* , 31 August 2022.

[3] D. Henke, N. Kelly, K. Marshall, I. Wevers and L. B. G. Knee, "A Turnstile Quad-Ridge Orthomode Transducer (OMT) for Octave-Bandwidth Receiver Front-Ends (24–51 GHz)," *in IEEE Transactions on Microwave Theory and Techniques*, vol. 71, no. 11, pp. 4906-4921, 2023.

[4] N. Tasouji, S. Salem Hesari, T. Sieverding and J. Bornemann, "High efficiency octave band feed horn antenna for radio astronomy applications," in *URSI International Symposium on Electromagnetic Theory*, Vancouver, BC, Canada, May, 2023.

[5] N. Tasouji, D. Henke, T. Sieverding, S. Salem Hesari, J. Bornemann and A. Densmore, "Design of Octave-Band Magic-T Using Stepped Ridges and Posts," in *33nd IEEE International Symposium on Space THz Technology (ISSTT 2024)* , Charlottesville, Virginia, US, 2024.

[6] J. W. Kooi and et al., " A Multioctave 8 GHz − 40 GHz Receiver for Radio Astronomy," *in IEEE Journal of Microwaves*, vol. 3, no. 2, pp. 570-586, April 2023.

[7] K. Jeganathan and et al., "Ultra Wideband (UWB) Receiver for Radio Astronomy," in *2019 International Conference on Electromagnetics in Advanced Applications (ICEAA)*, Granada, Spain, 2019.

[8] S. Manafi, M. Al-Tarifi and D. S. Filipovic, "45–110 GHz Quad-Ridge Horn With Stable Gain and Symmetric Beam," *in IEEE Transactions on Antennas and Propagation*, vol. 65, no. 9, pp. 4858-4863, Sept. 2017.

[9] J. Flygare and M. Pantaleev, "Dielectrically loaded quad-ridge flared horn for beamwidth control over decade bandwidth — Optimization, manufacture, and measurement," *IEEE Trans. Antennas Propag.*, vol. 68, no. 1, p. 207 – 216, Jan. 2020.

[10] A. Dunning, M. Bowen, M. Bourne, D. Hayman and S. Smith, "An ultra-wideband dielectrically loaded quad-ridged feed horn for radio astronomy," in *in Proc. IEEE-APS Top. Conf. Antennas Propagat. Wireless Comm.*, Feb. 2015.

[11] S. Salem Hesari, D. Henke, V. Reshetov, B. Veidt, A. Seyfollahi, F. Jiang and L. B. G. Knee, "Design and analysis of the NRC Q-band receiver for ngVLA Band-5," in *Proc. SPIE 12190, Millimeter, Submillimeter, and Far-Infrared Detectors and Instrumentation for Astronomy XI, 121900L*, 31 August 2022.

[12] S. Salem Hesari, D. Henke and L. B. G. Knee, "A Proposed Vacuum Window for DVA-2 Q-band receiver and ngVLA Band-5," in *2021 XXXIVth General Assembly and Scientific Symposium of the International Union of Radio Science (URSI GASS)*, Rome, Italy, , 2021.

[13] R. Selina and D. Dunbar, "System Reference Design," Nat. Radio Astron. Obs. NRAO Doc. 020.10.20.00.00- 0001-REP-B-SYSTEM_REFER-ENCE_DESIGN, ngVLA Ref. Des. , doi: 020.25.00.00.00-0001-REQ-A-ANTENNA_PRELIM_TECH_REQS., July 2019.

[14] C. A. Balanis, Antenna Theory: Analysis and Design, 3rd Edition, Wiley-Interscience, 2005.

[15] K. Pontoppidan, "Electromagnetic properties and optical analysis of the ALMA antennas and front ends," Nat. Radio Astron. Observatory, ALMA EDM Doc. FEND- 80.04.00.00-026-A-REP, Charlottesville, VA, Jan. 2008.

[16] D. Henke, S. Salem Hesari and L. B. G. Knee, "Axial Ring Feed Horn with Logarithmic Flare for Offset Gregorian Optics," in *in 2021 XXXIVth General Assembly and Scientific Symposium of the International Union of Radio Science (URSI GASS)*, Rome, Italy, 2021.

[17] S. Salem Hesari, D. Henke and L. B. G. Knee, "A Proposed Vacuum Window for DVA-2 Q-band receiver and ngVLA Band-5," in *URSI GASS 2021*, Rome, Italy, 28 August - 4 September 2021.

[18] S. Salem Hesari, D. Henke, B. Veidt, V. Reshetov and L. B. G. Knee, "A Compact Axial-Ring Feed Horn and Vacuum Window Model for a Cryogenic Q-band Receiver," in *2021 IEEE 19th International Symposium on Antenna Technology and Applied Electromagnetics (ANTEM)*, Winnipeg, MB, Canada, 2021.